



Using an Active Gurney Flap to Modify the Performance of a Wind Turbine Wing Section

Siyang Hao

*Center for Fluid Mechanics, School of Engineering, Brown University
Providence, RI, 02912, USA*

John Cooney

Arctura, Inc., South Kingston, RI, 02879, USA

Neal Fine

Arctura, Inc., South Kingston, RI, 02879, USA

Kenneth Breuer

*Center for Fluid Mechanics, School of Engineering, Brown University
Providence, RI, 02912, USA*

We report on the design, fabrication and testing of a wind tunnel model based on the geometry of a commonly-used wind turbine blade and the changes in aerodynamic performance of the wing due to the deployment of an active Gurney Flap (AGF). The AGF is located near the trailing edge of the wing on the pressure surface and is raised and lowered to modulate aerodynamic performance. The torque required to raise and lower the AGF was measured and found to be approximately $C_T = 0.1$, independent of deployment rate, and Reynolds number. Lift and Pitching moments of the wing with and without the AGF were measured over a range of angles of attack and at Reynolds numbers varying from 160,000 to 414,000. We find that the Gurney flap increases the lift and pitching moment of the wing over a wide range of Re and angles of attack.

I. Introduction

With the growth in utilization of wind energy, wind turbine technology has advanced rapidly in recent years and wind turbines have both grown in size, and improved their overall efficiency, such that modern turbines can now generate over 10 MW of power [1]. Improvements in turbine technology are still an area of focus, and one topic of active development is the ability to modulate the lift generated by the blade in response to unsteady atmospheric conditions (gusts) as well as periodic perturbations generated, for example, by the blade passing the support tower. Such load alleviation could lead to reduced Operations and Maintenance (O&M) costs and increased longevity for a given rotor design, or permit larger rotor diameters for a constant load envelope, thereby increasing energy capture. Lift modulation could also be used to supplement active blade pitch systems for future ultra-large machines.

Active flow techniques to achieve active load control have been proposed and tested and include the use of synthetic jets [2] and plasma actuators [3] as means to control boundary layer separation and overall aerodynamic force generation [4]. An alternative approach that seems promising is the use of a small vertical tab known as a Gurney flap [5]. The Gurney flap is a small piece of flat plate installing at the trailing edge of the pressure-side of a wing. This device was pioneered by American racing icon Dan Gurney on the rear wing of his racing car. The Gurney flap was soon adopted by not only the automobile industry but also in the aerospace field, for its ability to improve the lift-drag ratio [6, 7]. The use of a static Gurney flap on wind turbine blade geometries has also been explored [8] before with promising results.

Here we explore the idea of an active Gurney flap (AGF) - one that can be raised and lowered dynamically as the blade rotates, and thus provide real-time control of the aerodynamic and structural loads on the turbine blade. The objective of the current experiment is twofold: first, we are interested in determining the torque required to deploy the Gurney flap. Second, we are interested in the overall effectiveness of an active Gurney flap on the aerodynamic performance of a typical wind turbine blade. To address the first question, we installed a Gurney flap in the wind tunnel towards the back of a 1 meter long flat plate. The torque required to raise and lower the gurney flap was measured at several wind speeds and at several deployment rates. To address the issue of aerodynamic performance, a wing model

was built and the lift and pitching moments of the wing measured at several angles of attack, and Reynolds numbers.

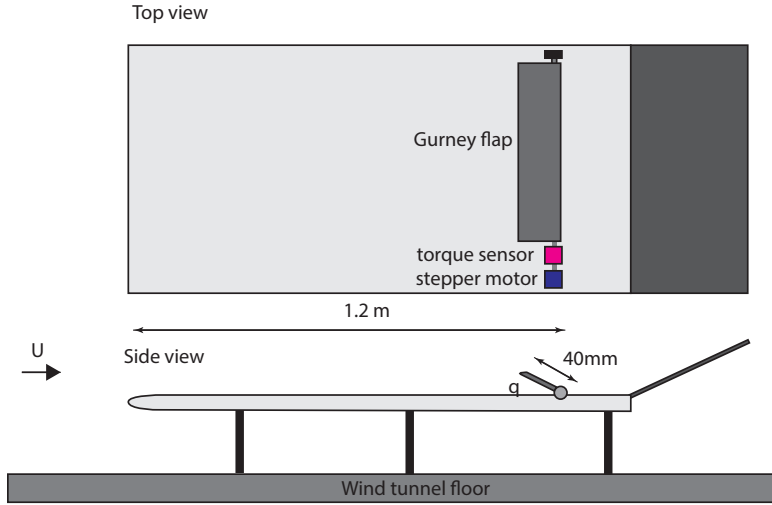


Fig. 1 Schematic of the flat plate wind tunnel model used to measure the torque required to rotate the Gurney flap.



Fig. 2 Setup. Left: CAD rendition of the test wing. The flow is from left to right. The wing is made from five interchangeable 3D-printed segments, labelled A-E, each 200 mm in width, and mounted onto two rectangular aluminum spars that span the entire wing from tip to tip. The overall span to the model is 1000 mm (exclude the endplate and outside structure). The center segment (C) holds a steel mounting bracket which clamps over the wing spars and connects to the sting, which itself is integrated with an internal six-axis force/torque transducer. In the configuration shown on the right end (E) holds the Scanivalve pressure transducer, while segment D has pressure taps for surface pressure measurements. Right: The model is installed in the wind tunnel, mounting on a pitch-yaw mechanism. The motor to control the Gurney flap can be seen on the outside of the left-side endplate. The driving and supporting mechanisms are also shown in the figures.

II. Experimental Details

A. Flat plate model

A 1.5m (streamwise) by 1.2m (spanwise) wooden laminate plate was used to test the torque required to deploy the Gurney flap in a flow (Fig. 1). The plate was made of 12 mm (1/2")-thick wood, had an angled leading edge and was installed 33 cm above the floor of the wind tunnel test section. A hinged flap, 30 cm long (in the streamwise direction) and spanning the test section width, was attached to the back, and adjusted so that the attachment streamline at the leading edge was on the upper surface. Although the plate surface was smooth, it was not polished, and this ensured that

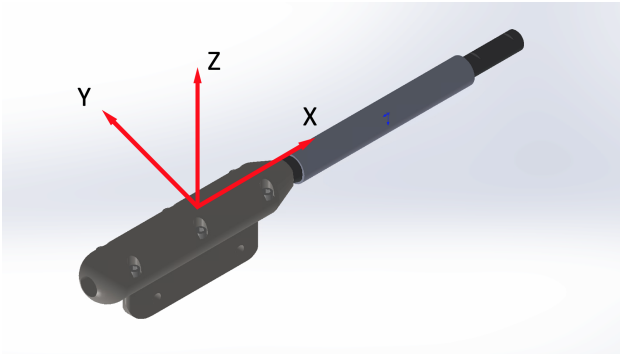


Fig. 3 Coordinate axis of the sting load cell.

a turbulent boundary layer was easily established on the upper surface of the plate.

A 600mm by 40mm gurney flap was installed 1.2 m downstream from the leading edge. The flap was supported by bearings so that it was free to rotate between 60 (tilting slightly forward) to 180 degrees (lying flap, tip facing downstream); 90 degrees implies that the flap was perpendicular to the plate surface. A torque transducer was mounted between the driving motor and the flap mechanism, and used to measure the time-varying and steady reaction torque experienced during actuation. Measurements were taken at two freestream velocities: $U_o = 20$ and 30 m/s, corresponding to Reynolds numbers based on the distance from the leading edge, $Re_x = 1,588,000$ and 2,382,000.

B. Wing model design and fabrication

A test model was designed to measure the aerodynamic forces experienced by a wind turbine blade with the use of an active Gurney flap. The model is two-dimensional (constant span, zero twist) with a geometry based on the profile of a Vestas V27 wind turbine blade at the spanwise location of maximum thrust loading. The wind tunnel model has a 1000 mm span and 250 mm chord and is comprised of five interchangeable wing segments each 200 mm wide (Fig 2). The wing segments are 3D printed by Selective Laser Sintering method (SLS) using Nylon, which provides a balance between surface quality, mechanical strength and geometric precision. An interchangeable socket on the end of each segment enables the wing to be assembled in any order, and for different wing segments to be easily swapped in and out.

The Gurney flap is comprised of two aluminum blades, each 10 mm high (4% chord), spanning one half-span. The blades are connected to a shaft and bearings and mounted on the pressure side of the wing at 96 % chord. The gurney flap is driven by a stepper motor positioned on the outside of the wing end plate. The control and power module for the gurney flap motor are housed in segment A of the wing.

Segment B is a general wing segment with no devices inside. A Scanivalve pressure transducer, used to measure pressure distributions across the wing, is embedded in segment E. The Scanivalve ports are connected to the surface pressure taps, located in segment D with flexible plastic tubing.

The entire structure, including the segments and end plates, are supported by two rectangular aluminum beams that span the entire wing. A CNC-machined steel clamp, located in segment(C), is used to attach the assembly to a mounting sting, which is instrumented with a six-axis force/torque transducer (Fig 3). The entire structure is supported by a motion control mechanism which adjusts the pitch and yaw angles of the model.

C. Instrumentation and data acquisition

Force data and pressure distributions of the wing model are collected during the experiment for each flow condition. The wind tunnel is first set to a free stream velocity, corresponding to a specific Reynolds number. The motion control mechanism pitches the model through a series of angles of attack. At each angle, the force and torque data is measured at 10 Hz for 5 seconds. The forces are averaged and corrected for the sting angle to generate the aerodynamic forces and torques. This sequence was repeated twice: first with the Gurney flap deployed at ninety degrees, then with the gurney flap lying flat on the wing surface. The pressure distribution was measured from the 27 pressure ports using a Scanivalve pressure transducer sampling at 10 Hz for 50s.

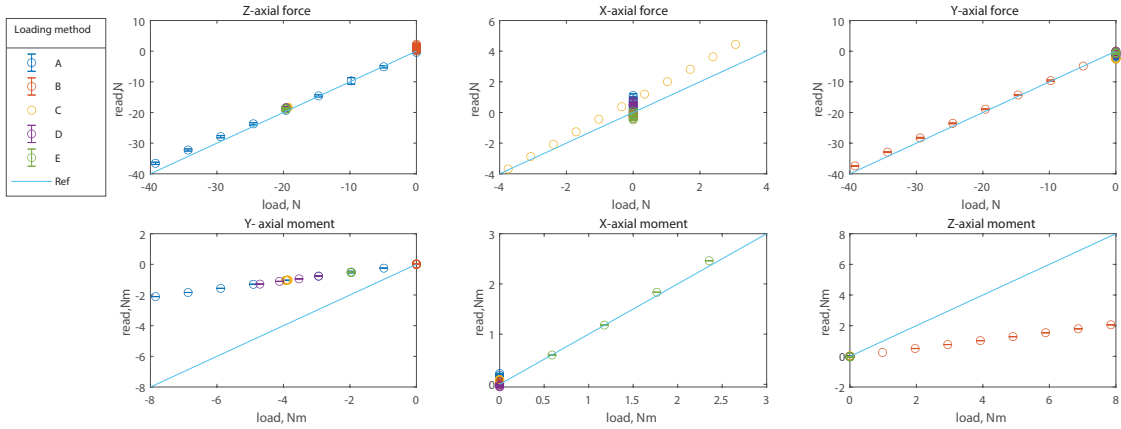


Fig. 4 Calibration of the sting load cell. Different loading methods are used to cover the six axis reading.

D. Calibration

A calibration was conducted to validate the accuracy of the force and torque data for the wing model. Five loading methods were applied to cover the force readings, F_x , F_y , F_z , and the corresponding moments. The loading methods used were:

- A Loading in the z -direction at a fixed position on the X -axis. This generates a normal (z -direction) force and a pitching (y -direction) moment;
- B Loading in the z -direction, at a fixed position on the x -axis, and with the load offset by a fixed length in the y axis. This generates a load in the z -direction, as well as a pitch (y) and roll (x) moment.
- C Loading at a fixed position on the x -axis, with the loading weight hanging downwards. By rotating the sting by angle θ with respect to gravity, the forces in (x , z) directions are given by $(\sin \theta, \cos \theta)$ respectively, while the pitching moment varies like $\cos \theta$.
- D Identical to method A, but with the load placed at a different position on the x -axis. This generates a force in the z -direction but a different pitching (y -direction) moment;
- E Identical to method B, but with the load placed at a different position on the x -axis, generating a similar fixed z -direction force but different x -direction moment.

The calibration (Figure 4) validates the three-axis force readings and x -moment readings with loading.

One concern is that the y and z -moment readings appear to be one quarter of actual values. This is corrected in the data presented, but needs to be clarified in a second series of experiments.

III. Results

A. Flat Plate model results

The torque coefficient, $C_T = T / 0.5 \rho U^2 h$, where T is the torque, ρ and U , the air density and speed, and h the length of the Gurney flap, is shown for different flap deployment angles and different Reynolds numbers in Figure 5a. Zero degrees indicates that the flap is pointing upstream, while 180 degrees indicates that the flap is pointing downstream. In general the torque coefficient is independent of Reynolds number (Figure 5a). The lowest torque is observed when the flap is lying flat, pointing downstream (angles close to 180°), while the highest torque occurs when the flap is vertical (90°). It remains approximately constant as the flap pitches forward. The torque coefficients were not found to be sensitive to the deployment rate which was varied from 9 degrees per second to as high as 180 degrees per second. (Figure 5b). The maximum torque observed, $C_T \sim 0.1$ is lower than, but comparable to, the torque coefficient of 0.25 which would be experienced by a flat plate of height h exposed to the dynamic pressure ρU^2 associated with a uniform velocity, U_o . If one assumes a model turbulent boundary layer, $U(y) \sim U_o(y/h)^{1/7}$ [9], the theoretical prediction changes only slightly, to $C_T = 7/15$. The lower value of C_T measured here is due to the back-pressure behind the flap which provides some additional torque relief.

A significant vibration was observed when the flap was pointing downstream, and this was found to be caused by

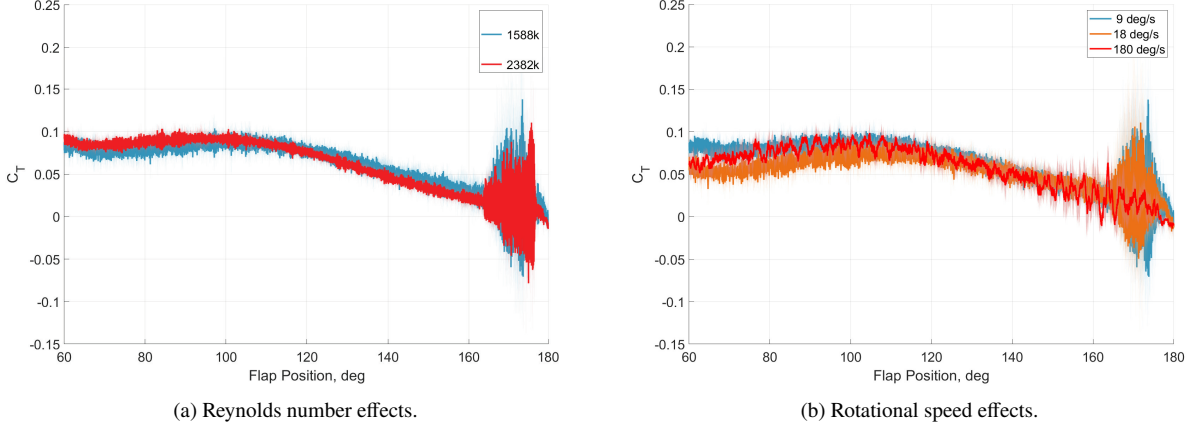


Fig. 5 Torque vs angle during Gurney flap deployment. The Torque coefficient, C_T , is shown as the flap is moved between 60 degrees (flap facing upstream through 180 degrees (flap lying flat, facing downstream). Left: C_T at two Reynolds numbers, Re_x . Right: C_T at $Re_x = 1,588,000$ at different rotational speeds. Right: C_T at three different deployment speeds.

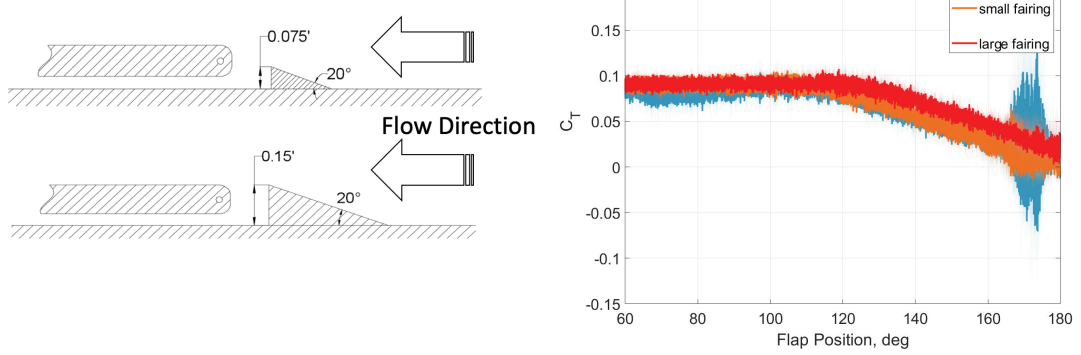


Fig. 6 Torque vs angle during Gurney flap deployment with and without the anti-vibration fairing. Re number $Re = 1,588,000$.

vibration initiated by the boundary layer that had grown on the flat plate impinging on the transition to the flap. The vibration was found to be alleviated by placing a small fairing with a 20 degree wedge immediately upstream of the flap. The wedge diverted the boundary layer flow and completely eliminated the vibration, but did not change the overall torque characteristics (Fig 6).

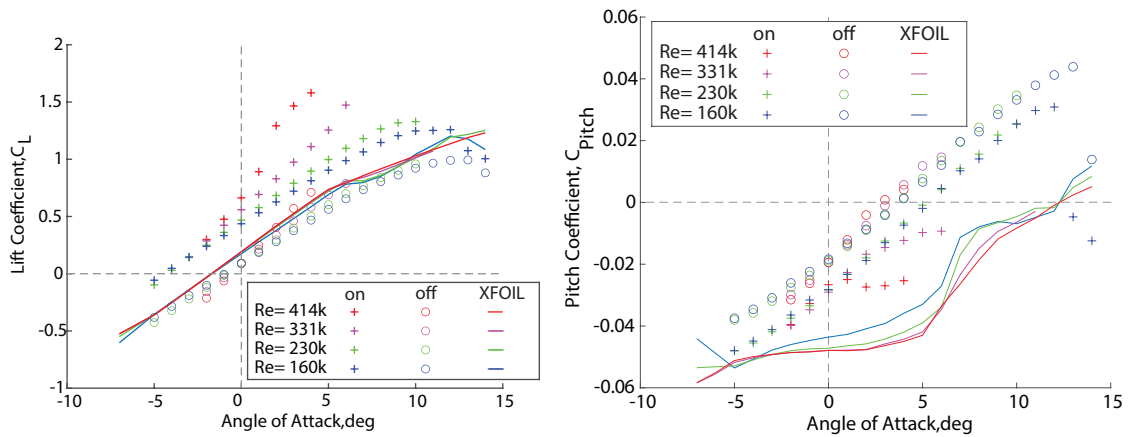


Fig. 7 Lift coefficient, C_L , (left) and Pitch coefficient, C_M , (right) as a function of angle of attack, α , at four different Reynolds numbers. Circles represent data with the flap stowed parallel to the wing surface (off). Crosses represent data with the flap deployed at 90° (on).

B. Lift and Pitch coefficients of the wing

Lift, C_L , and Pitch coefficients, C_M of the wing with the AGF system are presented as a function of angle of attack, α , in Fig 7. The effect the Gurney flap is evident, resulting in an increase in the Lift coefficient and a shift towards more negative pitch coefficients over all angles of attack. More subtle variations are also observed at different Reynolds numbers. Note that, at higher values of Re , the tests could not be conducted at high angles of attack due to the fact that the forces exceeded the range of the force transducer. As the Reynolds number increases, the lift slope, $dC_L/d\alpha$, increases, and the slope increment is more pronounced for the case of the deployed flap configuration. This results in a larger lift enhancement due to the Gurney flap deployment at the higher Reynolds numbers and angles of attack.

There is no discernible Re -effect on the pitching moment, C_M , for the baseline wing. However, when the flap is raised, the higher Reynolds number cases trend towards a plateau in (negative) C_M , which occurs earlier and at a more negative value as the Reynolds number increases.

C. Surface Pressure

Surface pressure measurements across the wing model are shown in Figure 8. Pressure on the upper (suction) surface is shown in red while pressure on the lower (pressure) surface is shown in blue. Measurements were taken at two Reynolds numbers, $Re = 160k$ and $230k$ (upper and lower rows respectively in Fig 8). The solid lines are computed pressure distributions, computed using XFOIL [10]. For the undisturbed, clean wing, the agreement between the measured and predicted pressure distributions is generally quite good, with some discrepancies at approximately 70% chord where the separation bubble closes and the wing reattaches.

It is evident that the Gurney flap does have a significant effect on the pressure distribution, but that there does not seem to be a significant effect due to Reynolds number. Deploying the flap does affect the pressure distribution,

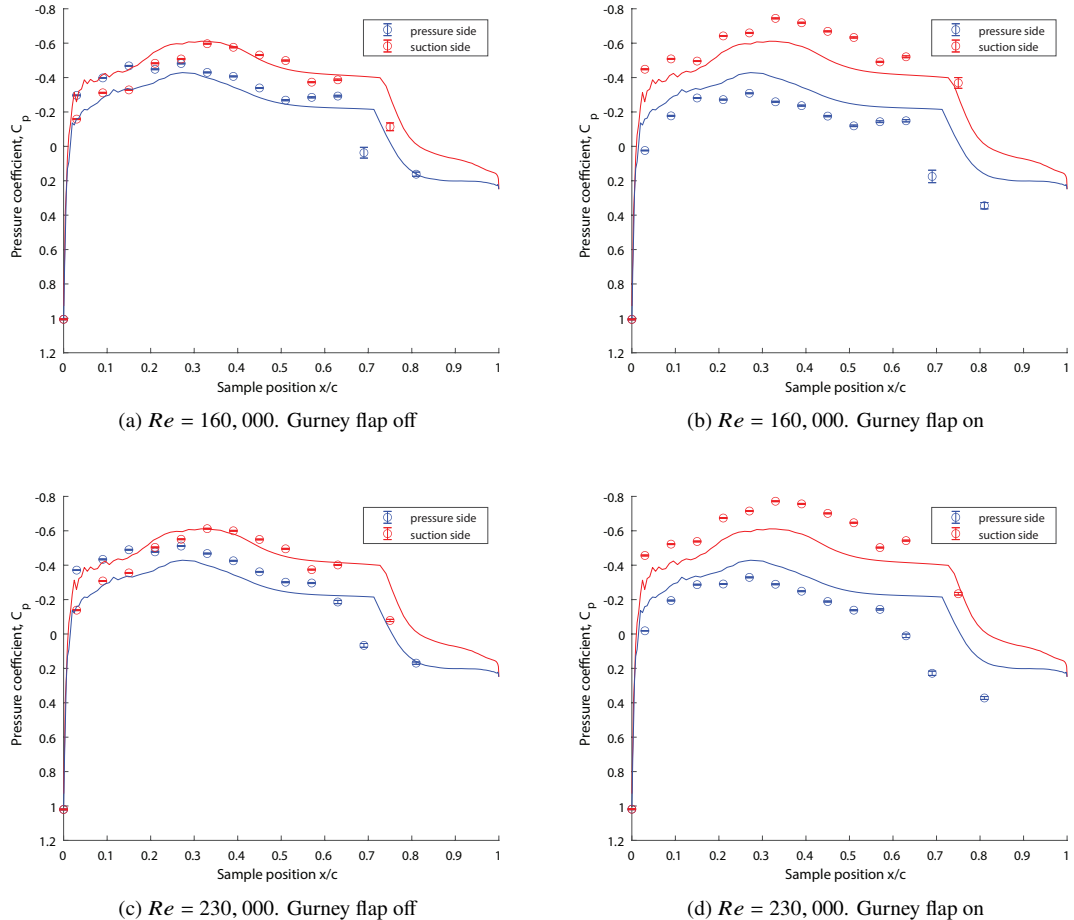


Fig. 8 Pressure distribution on the airfoil with gurney at $Re = 160,000$ (Top Row) and $Re = 230,000$ (Bottom Row) at zero degrees angle of attack. The solid lines from the XFOIL computation of a 2D bare wing are shown for reference. The pressure distribution is measured from the pressure taps on both pressure side (blue) and suction side (red) of the airfoil. With gurney flap at off position, the pressure distribution shows a good agreement of predictions. When the gurney flap is turned on, the pressure increased on the pressure side and decreased on the suction side.

generating stronger suction on the upper surface, at a slightly more aft location on the wing. From the shape of the pressure distribution on the lower surface, it also appears that the separation bubble on the lower surface closes a little earlier and that a stronger (less negative) pressure recovery is achieved towards the trailing edge. Both of these effects contribute to the increased lift coefficient and the increased pitching coefficient described earlier (Fig. 7).

IV. Discussion and Conclusions

Although these results are still somewhat preliminary, there is good evidence that the Gurney flap holds significant promise for controlling both the lift and pitching moment on a wind turbine blade during operation. The torques required for deployment are modest, and seems well behaved - a necessary requirement for robust control in the challenging environment of a commercial wind turbine. More importantly, the lift forces are significantly enhanced by the deployment of the flap, although there are also changes in the pitching moment that will need to be accounted for in both the blade control and the prediction of structural support of the wing.

This experimental campaign represents a first step, and there are several things that need to be improved, repeated and expanded upon. Ongoing work includes:

- Re-calibration of the force balance - there were some inconsistencies in the calibration of the pitching moment that need to be investigated further and confirmed.
- More pressure measurements at more angles of attack.
- Dynamical measurements of the lift and pitching moment to understand quickly the forces adapt as the flap is deployed. This is well within our experimental capabilities, but was not completed due to lack of resources.

V. Acknowledgements

This work was conducted with financial support from the Rhode Island Commerce Corporation (RICC), through the Innovation Voucher Program.

References

- [1] GE, “GE Wind Energy Solutions,” , 2021. URL <https://www.ge.com/renewableenergy/wind-energy>.
- [2] Glezer, A., and Amitay, M., “Synthetic Jets,” *Annual Review of Fluid Mechanics*, Vol. 34, No. 1, 2002, pp. 503–529. <https://doi.org/10.1146/annurev.fluid.34.090501.094913>.
- [3] Brownstein, I. D., Slateniyi, C., and Breuer, K. S., “Enhanced Aerodynamic Performance of a Wind Turbine Airfoil Section Using Plasma Actuation,” *52nd Aerospace Sciences Meeting*, American Institute of Aeronautics and Astronautics, National Harbor, Maryland, 2014. <https://doi.org/10.2514/6.2014-1244>.
- [4] Aubrun, S., Leroy, A., and Devinant, P., “A Review of Wind Turbine-Oriented Active Flow Control Strategies,” *Experiments in Fluids*, Vol. 58, No. 10, 2017, p. 134. <https://doi.org/10.1007/s00348-017-2412-0>.
- [5] Wikipedia, 2021. URL https://en.wikipedia.org/wiki/Gurney_flap.
- [6] Maughmer, M. D., and Bramesfeld, G., “Experimental Investigation of Gurney Flaps,” *Journal of Aircraft*, Vol. 45, No. 6, 2008, pp. 2062–2067. <https://doi.org/10.2514/1.37050>.
- [7] Wang, J. J., Li, Y. C., and Choi, K. S., “Gurney Flap—Lift Enhancement, Mechanisms and Applications,” *Progress in Aerospace Sciences*, Vol. 44, No. 1, 2008, pp. 22–47. <https://doi.org/10.1016/j.paerosci.2007.10.001>.
- [8] Saenz-Aguirre, A., Fernandez-Gamiz, U., Zulueta, E., Ulazia, A., and Martinez-Rico, J., “Optimal Wind Turbine Operation by Artificial Neural Network-Based Active Gurney Flap Flow Control,” *Sustainability*, Vol. 11, No. 10, 2019, p. 2809. <https://doi.org/10.3390/su11102809>.
- [9] Kundu, P. K., Cohen, I. M., and Dowling, D. R., *Fluid mechanics*, 5th ed., Academic Press, 2012.
- [10] Drela, M., “XFOIL: An Analysis and Design System for Low Reynolds Number Airfoils,” *Low Reynolds Number Aerodynamics*, Lecture Notes in Engineering, Vol. 54, edited by T. J. Mueller, Springer, 1989.